

# Top squark signal significance enhancement by different Machine Learning Algorithms

Jorge Fraga<sup>\*</sup>, Ronald Rodriguez<sup>†</sup>, Jesus Solano<sup>‡</sup>,  
Juan Molano<sup>§</sup> and Carlos Ávila<sup>¶</sup>

*Department of Physics, Universidad de los Andes,  
Bogotá - Colombia.*

June 15, 2021

## Abstract

A study of four different machine learning (ML) algorithms is performed to determine the most suitable ML technique to disentangle a hypothetical supersymmetry signal from its corresponding Standard Model (SM) backgrounds and to establish their impact on signal significance. The study focuses on the production of SUSY top squark pairs (stops), in the mass range of  $500 < m_{\tilde{t}_1} < 800$  GeV, from proton-proton collisions with a center of mass energy of 13 TeV and an integrated luminosity of  $150 \text{ fb}^{-1}$ , emulating the data-taking conditions of the run II LHC accelerator. In particular, the semileptonic channel is analyzed, corresponding to final states with a single isolated lepton (electron or muon), missing transverse energy, and four jets, with at least one tagged as  $b$ -jet. The challenging compressed spectra region is targeted, where the stop decays mainly into a  $W$  boson, a  $b$ -jet, and a neutralino ( $\tilde{t}_1 \rightarrow W + b + \tilde{\chi}_1^0$ ), with a mass gap between the stop and the neutralino of about 150 GeV. The ML algorithms are chosen to cover different mathematical implementations and features in machine learning. We compare the performance of a logistic regression (LR), a Random Forest (RF), an XGBoost (XG), and a Neural Network (NN) algorithm. Our results indicate that all four algorithms provide an improvement in signal significance calculation when compared to the ones obtained with a standard analysis method based on sequential requirements of different kinematic variables. The highest gain in significance is obtained with the NN and XG classifiers with an average improvement over 20%, both having compatible statistical performance for the stop mass range considered, followed by RF(15%). The LR has the poorest performance of all ML algorithms studied, but still presents an average improvement of about 4%.

---

<sup>\*</sup>Email: jf.fraga@uniandes.edu.co

<sup>†</sup>Email: rrodriguez@uniandes.edu.co

<sup>‡</sup>Email: ja.solano588@uniandes.edu.co

<sup>§</sup>Email: jp.molano56@uniandes.edu.co

<sup>¶</sup>Email: cavila@uniandes.edu.co

# 1 Introduction

The popularity of Machine Learning (ML) algorithms have expanded to different areas of knowledge, leaning in the last decade to Deep Learning algorithms [1, 2]. In the field of High Energy Physics (HEP), ML algorithms have been used in different experimental searches, for instance, in particle reconstruction and identification [3–8], physics measurements [9–11], and fast data processing [12, 13]. The Large Hadron Collider (LHC) experiments have been applying different ML techniques to analyze and extract relevant information from the large amount of data collected by each specific detector [14]. Some of the most common approaches are neural networks, support vector machines, random forest, boosted decision trees (BDT), and others [15]. Many of these algorithms are mainly used for identifying and recording data related to the physical properties of particles, for example, in particle path reconstruction based on the information collected by tracker detectors and jet identification in hadronic calorimeters [16]. Additionally, ML algorithms are extensively involved in the optimization of data storage and information flow in the computing GRID centers worldwide [17, 18]. Moreover, the implementation of ML algorithms played an important role in the discovery of the Higgs Boson in 2012 [19, 20], where the analyses were performed using BDTs.

In this study, four ML algorithms are implemented with the purpose of discriminating SM backgrounds from beyond Standard Model (BSM) hypothetical processes in order to maximize the significance. We compare this approach to traditional analyses based on event cut-and-count methodologies. To accomplish this goal, a case of study in the search for SUSY particles is proposed, focusing on the production of stop pairs in proton-proton collisions at 13 TeV in the LHC environment. Particularly, we look for stops with R-parity conservation with mass points along the so-called compressed scenario where the difference between the mass of the stop and the neutralino is smaller than the mass of the on-shell top quark [21–23].

This article is structured as follows. Section 2 contains a brief introduction to the current searches of SUSY stop particles in the LHC and introduces the ML algorithms used in the present investigation. Section 3 provides all the details related to the MC sample generation used for the current study and describes the two strategies whose performance is compared: the signal extraction using standard methodologies based on event cut-and-count and the signal extraction using ML algorithms. For the latest method, the kinematic features and the structure of the data sets used for training and evaluation are also specified. The results of the performance of both strategies are presented in section 4. Additionally, for the ML algorithms, a comparative analysis is performed based on classification metrics and a significance optimization for each signal benchmark. A comparison of signal significance obtained by the four ML classification algorithms and the standard classical method is made in terms of the gain in significance obtained from each analysis. Finally, conclusions are drawn in section 5.

## 2 Search for SUSY stop particles

Despite its mathematical rigor and precise predictions, the SM of particle physics does not provide a complete description of nature. It still presents several shortcomings such as being unable to provide any explanation for neutrino masses [24], the nature of dark matter [25] and dark energy [26], the strong CP violation [27], among others. Additionally, The SM also runs into quadratic divergences from top quark loop corrections in the Higgs mass Feynman diagrams [28, 29], known as the hierarchy problem [30].

Supersymmetry (SUSY) is one of the most popular hypothesis to search for physics BSM,

since it works as an extension of the SM, requiring an additional symmetry between fermions and bosons [31]. Within SUSY, some variants assume different couplings and free parameters, which determine how this symmetry is broken and the mass spectra of the supersymmetric particles [32–36]. A relevant particle when looking for signatures of SUSY is the squark top  $\tilde{t}_1$  (stop), since its existence could imply a natural solution to the hierarchy problem [37]. As the stop is the super-partner of the top quark, its positive contribution to the Higgs mass corrections cancels out naturally the largest negative diverging contribution coming from the SM top quark. Additionally, in most SUSY models with R-parity conservation, the lightest supersymmetric particle is the neutralino  $\tilde{\chi}_1^0$ , which arises naturally as a strong candidate for dark matter, due to its large mass, weakly interactive nature, and extended lifetime [38].

This study explores the production of pairs of SUSY stop particles from proton-proton collisions in a compressed spectra scenario, where the mass difference between the top squark and the lightest neutralino is smaller than the top quark mass by about 20 GeV, causing the particles of the final state to have very low kinetic energy [21–23]. In this case, each stop decays dominantly to an off-shell top quark and a neutralino, with the top quark subsequently decaying into an on-shell  $W$  boson and a  $b$ -quark. The two neutralinos in the final state are usually produced in opposite directions, generating a very low missing transverse momentum in the event, increasing the experimental challenge to distinguish the SUSY signal from its SM backgrounds.

There are three final state topologies in the direct stop pair-production, depending on how each  $W$  boson in the final state decays: the full hadronic, semileptonic, and dileptonic channels. This study focuses in the semileptonic channel, where one of the  $W$  bosons decays into quarks and the second one into a charged lepton (electron or muon) and a neutrino ( $W \rightarrow \ell\nu$ ), corresponding to events with final states with a single isolated lepton, missing transverse momentum, and four jets with at least one of them tagged as a  $b$ -jet. An important advantage of this specific topology is the reduction of QCD background due to the requirement of the isolated lepton [39, 40]. A detailed Feynman diagram of this process is shown in Figure 1.

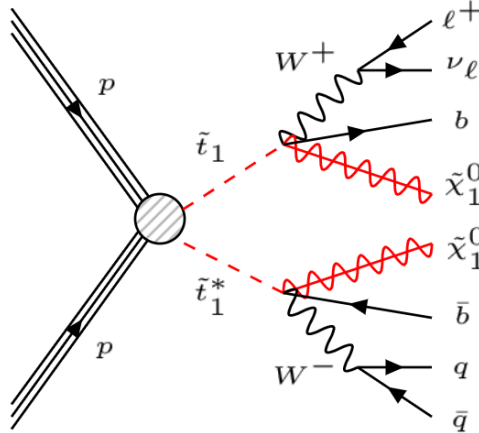


Figure 1: Feynman diagram for stop pair production with three body decay and semileptonic final states, with  $\ell = e, \mu$ .

So far, searches by CMS and ATLAS experiments for stops in the semileptonic channel have yielded null results and established exclusion limits for the stop mass up to about 1 TeV

and for neutralino masses approximately below 600 GeV [41, 42].

ML methods are by now a well-established framework in most HEP experiments to improve the performance in the detection of particles, analyzing in principle all multiple correlations between their features [3, 4, 9, 10]. In the last decade, the improvement of ML algorithms implied for instance larger and more robust neural networks, with many hidden layers and nodes. These improvements have increased the capabilities to extract deeper and meaningful information from the combination of several features of the large amount of data stored by any specific experiment at the LHC [43, 44]. The use of ML algorithms has been rapidly extended to the analysis of phenomenological and experimental studies, for example, in searches of new physics phenomena such as anomaly detection or the decay of hypothetical Supersymmetric particles [45–49]. ML algorithms have already been used in the search for stop production to discriminate final decay products from SM backgrounds. In reference [41], the ATLAS experiment reports an analysis for the production of pairs of stops in the semileptonic channel using a recurrent neural network to reduce jet multiplicity and a shallow neural network to perform the discrimination between SUSY signals and backgrounds. The present study expands and improves this type of analysis with the implementation of neural networks with more hidden layers and neurons to improve the training, and by making a comparison with additional ML algorithms in order to determine the one with the highest performance in enhancing signal significance for top squark masses up to 800 GeV via the three-body decay ( $\tilde{t} \rightarrow bW\tilde{\chi}_1^0$ ).

The effectiveness to discriminate SM backgrounds from stop decay processes is investigated for the following ML algorithms: a Logistic Regression [50], which basically estimates the conditional probability of a dichotomous variable by fitting the model parameter using maximum likelihood; a Random forest [51] classifier, which constructs many different decision trees that classify a sample by majority voting; a Gradient Boosting [52] (XGBoost) classifier, which is an ensemble method which sequentially improves a base decision tree by means of optimizing a loss function; and finally, a sequential neural network [53] (NN) classifier, which includes multiple hidden layers and neurons to encode non-linear relationships between inputs and outputs. It is important to remark that the selection of these specific classifiers was aimed to have a wide range of models increasing in complexity. Note that the features behind the proposed classifiers are different which let us understand and choose the best approach to our task.

## 3 Event samples and search strategies

### 3.1 Event samples

MC samples of signal and background events are generated following similar criteria as previous experimental searches of production of stop pairs from proton collisions at the LHC. Samples are generated at leading order in the matrix elements for proton-proton collisions with a center of mass energy of 13 TeV. For the hard collisions at parton level, we use Madgraph 5 [54, 55], and Pythia 8 [56] for showering and hadronization simulation. Finally, the detector simulation has been implemented in Delphes [57], using the anti- $k_t$  clustering method and FastJet [58, 59], with a jet radius parameter of  $R = 0.5$ , where  $R = \sqrt{\eta^2 + \phi^2}$  with  $\eta$  the pseudorapidity and  $\phi$  the azimuthal angle. For b-tagging,  $E_T^{miss}$ , and lepton identification efficiency, we use the parameters established in Delphes to simulate the performance of the CMS detector [60].

## SUSY Signal

The signal sample parameters are produced using the SoftSusy package [61] based on the Minimal Supersymmetric Standard Model (MSSM). A large scan over the MSSM parameters is performed to look for signal signatures lying along the compressed mass spectrum. In our study we require that the difference in mass between the stop and the lightest neutralino to be around 150 GeV. We have selected four signal benchmark mass points taken into account the NNLO-NLL cross-sections [62]. Other parameters of the benchmarks selected are shown in Table 1, where the notation *s500* names the benchmark with stop mass of 500 GeV, and so on. This notation is used throughout this article to refer briefly to our signal benchmark points.

Table 1: MSSM signal parameters for each benchmark in the present study.

Parameters	<i>s500</i>	<i>s600</i>	<i>s700</i>	<i>s800</i>
$m(\tilde{t})$ [GeV]	500	600	700	800
$m(\tilde{\chi}_1^0)$ [GeV]	350	450	550	650
$\sigma$ (NNLO-NLL) [ $\text{fb}^{-1}$ ]	0.6090	0.2050	0.783	0.0326
$\Omega h^2$	2.94	5.34	5.97	8.74
$m_0$ [GeV]	2450	2600	2560	2400
$m_{1/2}$ [GeV]	800	950	1240	1400
$A_0$ [GeV]	-5950	-6500	-7200	-7300
$\tan \beta$	25	25	35	32

## Backgrounds

For backgrounds, the processes shown in Table 2 are generated, which are the most representative for the channel under study, and consistent with other SUSY searches with a similar final state topology [41, 42]. Since the  $t\bar{t}$  process has a significant contribution, it has been divided into two channels, the semileptonic ( $t\bar{t}$  1L) and the dileptonic ( $t\bar{t}$  2L). The contribution from the hadronic channel becomes negligible after applying the pre-selection requirements discussed in the following section. Another significant background is  $W$ +jets, for which MC samples are produced after splitting it into three HT binned channels: 100-200, 200-400 and  $H_T > 400$  GeV, where HT is the scalar sum of the transverse momentum of the hadrons. The lower limit for HT of 100 GeV has been selected taking into account that there are four jets in the final state, whose scalar addition of transverse momentum is usually higher than this lower threshold. Another important background is the single top production. We take into account the three main decay channels:  $Wt$ ,  $s$ -channel, and  $t$ -channel. In the case of the latest channel, we have separated the  $t b j$  and  $t j$  final state production for convenience. We also consider the  $t\bar{t} + V$  production, where  $V = W, Z$ , and the diboson production channels:  $WW$ ,  $WZ$  and  $ZZ$ .

In our study, we have required all background processes that contain vector bosons ( $W, Z$ ) in their final states to decay to leptons ( $\ell = e, \mu$ ) at parton level, so a reduction in MC generated events is obtained by the smaller branching ratio of the decay to leptons. Scale factors have been applied to the background distributions to compensate the reduction of events with jets with respect to the inclusive processes. Additionally, NLO k-factors [63] have been applied to normalize all background distributions.

Table 2: LO cross-sections for SM backgrounds at  $\sqrt{s} = 13$  TeV.

Background	Sub-processes	$\sigma_{LO} \cdot BR[pb]$
$t\bar{t}$ 1L		136.1
$t\bar{t}$ 2L		20.09
$W$ +jets	$H_T \in [100, 200]$ GeV	51.89
	$H_T \in [200, 400]$ GeV	17.68
	$H_T \in [400, \infty]$ GeV	2.703
Single Top	$Wt$	13.16
	t-channel ( $tbj$ )	15.79
	t-channel ( $tj$ )	5.166
	s-channel ( $tb$ )	0.8814
$t\bar{t} + V$	$t\bar{t} + W$	0.3455
	$t\bar{t} + Z$	0.5856
Diboson	$WW$	9.849
	$WZ$	4.253
	$ZZ$	3.752

### 3.2 Event pre-selection for ML training

Following the expected final states from the Feynman diagram of Figure 1, we select events with only one lepton ( $\ell = e, \mu$ ) with  $p_T > 25$  GeV and  $|\eta| < 2.5$  to remain within the detector's acceptance and to take into account the plateau trigger efficiency of CMS and ATLAS experiments for very well reconstructed leptons. Additionally, these selections reduce the hadronic  $t\bar{t}$  and QCD multijet backgrounds. We require at least four reconstructed jets with  $p_T > 25$  GeV and  $|\eta| < 2.5$ , and at least one of these jets to be  $b$ -tagged. Following the analysis strategies reported in [41] and [42], to reduce QCD multijet background events, we require that the azimuthal angular difference between  $E_T^{miss}$  and the two leading jets to be greater than 0.4, to ensure an isolated missing transverse momentum vector.

After making these selections, the efficiency to accept  $W$ +jets background events is very low, as can be observed in the event flow supplied in Table 4. Note that the initial number of events of  $W$ +jets is more than four times the main background  $t\bar{t} + 1L$ . Additionally, the  $W$ +jets background has a large cross-section (see Table 2), implying a large number of events to be produced in order to satisfy the requirement of  $150 \text{ fb}^{-1}$ , to closely simulate the statistics collected by LHC experiments in Run II. So, in our study, this background constitutes a computational constraint.

On the other hand, we look for selections that enhance the discriminating capacity of the training features and at the same time keep the number of samples feasible for training. For this purpose, we optimize a selection in the transverse mass of the lepton and the missing transverse energy,  $m_T^{lep}$ , defined as:

$$m_T^{lep} = \sqrt{2p_T^\ell E_T^{miss}(1 - \cos \Delta\phi(E_T^{miss}, p_T^\ell))}. \quad (1)$$

This selection reduces backgrounds such as  $W$ +jets and  $t\bar{t}$  semileptonic since it reconstructs indirectly the  $W$  boson from the final states. Likewise, we optimize a selection on  $E_T^{miss}$  that comes mainly from the two energetic neutralinos in the final states of the signal events.

Considering the limitation in our computational capacity, we have found that selections of  $m_T^{lep} > 90$  GeV and  $E_T^{miss} > 90$  GeV allow us to generate a maximum of 400000 events for the ML training, divided equally as 50% events for signal and 50% for backgrounds. The left panel of Figure 2 shows the  $m_T^{lep}$  distribution after the basic topological selections mentioned above. The right panel of Figure 2 shows the  $E_T^{miss}$  event distribution after the 90 GeV selection on  $m_T^{lep}$ . A summary of the event pre-selections is shown in Table 3. A complete event flow for backgrounds and the signal benchmarks are presented in tables 4 and 5, respectively.

Finally, for evaluation, we have generated  $150 \text{ fb}^{-1}$  for all backgrounds except for  $W$ +jets background, where we have generated events only for an equivalent integrated luminosity of  $86.9 \text{ fb}^{-1}$  (given our computing limitations) and then scaled it to  $150 \text{ fb}^{-1}$ . This scaling affects the uncertainty of the final background estimation. For the signal benchmarks, in order to have smooth distributions we generate higher statistics and then scale it to same luminosity as background events.

Table 3: General pre-selection requirements.

$N(\ell)$ ( $\ell = e, \mu$ )	$=1$ ( $p_T > 25 \text{ GeV}$ , $ \eta  < 2.5$ )
$N(j)$	$\geq 4$ ( $p_T > 25 \text{ GeV}$ , $ \eta  < 2.5$ )
$N(\text{b-tag})$	$\geq 1$
$\min \Delta\phi(j_{1,2}, E_T^{miss})$	$> 0.4$
$m_T^{lep}$	$> 90 \text{ GeV}$
$E_T^{miss}$	$> 90 \text{ GeV}$

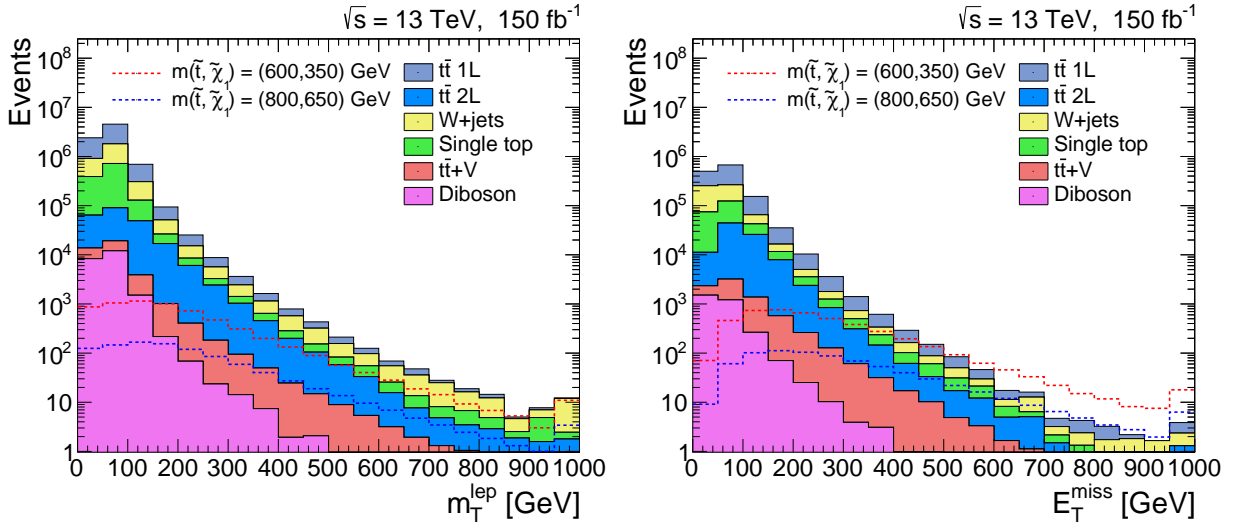


Figure 2: Distributions for transverse mass  $m_T^{lep}$  (left panel) before the 90 GeV selection and  $E_T^{miss}$  (right panel) after the  $m_T^{lep} > 90$  GeV selection.



Table 4: Event flow for backgrounds at a luminosity of 150 fb<sup>-1</sup>.

	Backgrounds						
	$t\bar{t}$ 1L	$t\bar{t}$ 2L	$W$ + jets	Single Top	$t\bar{t}$ + $V$	Diboson	Total
Initial Events	30125000	4388210	127770000	15363000	203125	3491520	181341000
$N(\ell = e, \mu) = 1$ ,	20022300	1922990	82344200	10673600	58541	1007900	116030000
$N(j) \geq 4$	16507400	854673	17146600	3955510	53474	128215	38645900
$N(\text{b-tag}) \geq 1$	6299440	257463	2263880	1313460	22800	12803	10169800
$\min \Delta\phi(j_{1,2}, E_T^{\text{miss}}) > 0.4$	5655100	231285	1948550	1161240	20130	11049	9027350
$m_T^{\text{lep}} > 90$ GeV	772242	85138	350959	164927	4916	1169	1379350
$E_T^{\text{miss}} > 90$ GeV	161609	43378	41903	30355	2431	161	279836

Table 5: Event flow for signal benchmarks with 50000 simulated events and scaled to a luminosity of 150 fb<sup>-1</sup>.

	Signal			
	$s500$	$s600$	$s700$	$s800$
Initial Events	91371	30748	11859	4852
$N(\ell = e, \mu) = 1$ ,	62019	20868	8011	3257
$N(j) \geq 4$	55052	18569	7116	2887
$N(\text{b-tag}) \geq 1$	22452	7601	2953	1206
$\min \Delta\phi(j_{1,2}, E_T^{\text{miss}}) > 0.4$	20712	7020	2735	1118
$m_T^{\text{lep}} > 90$ GeV	13146	4501	1797	752
$E_T^{\text{miss}} > 90$ GeV	11831	4091	1653	699

### 3.3 Signal extraction with a standard cut-and-count method

We use  $E_T^{\text{miss}}$  as a critical variable to look for any signature of stop production, since large  $E_T^{\text{miss}}$  is expected from neutralinos that cannot be detected in the final states (see Figure 1). As a consequence, we expect signal events with large values of  $E_T^{\text{miss}}$  compared to background processes. This can be verified in the left panel of Figure 2 for the  $s600$  and  $s800$  benchmark distributions, where the last bin that contains the tail events is enhanced. The strategy we are following is to make convenient selections on other kinematic variables to boost the significance in the final distribution of  $E_T^{\text{miss}}$ , and afterwards make particular selections in  $E_T^{\text{miss}}$  to maximize each benchmark significance.

The significance in our study is defined as

$$\text{Sig} = \frac{S}{\sqrt{S + B + 0.25B}}, \quad (2)$$

where  $S$  corresponds to the number of signal events and  $B$  the background events remaining after applying the event selection criteria. The factor  $0.25B$  is used to take into account, in a conservative way, an overall systematic uncertainty associated with the background estimation. Some sources of these uncertainties are related to the total contributions of theoretical and experimental uncertainties from the MC simulators to get the cross-sections and the particle reconstruction efficiencies, respectively [64]. Other sources are related with the jet energy scale (JES), jet energy resolution (JER),  $E_T^{\text{miss}}$ , lepton and b-tagging identification [65–67]. Our approach here is to consider an overall systematic uncertainty greater than the total systematic uncertainty values reported by the CMS and ATLAS experiments [41, 42].



Once all pre-selections are implemented, we proceed to optimize the significance in distributions of kinematic variables of signal and background events. The most representative distributions of these variables (normalized to unity) are shown in Figure 3, which correspond to the features chosen for ML training, since they exhibit different behaviour in signal as compared to overall background. To generate these plots, we have stacked every background in one single histogram, and for the signal we have stacked the four benchmark events together adding their contribution proportional to their cross section (see Table 1). We stack the signal samples this way for general comparison to their corresponding backgrounds, which help us to reveal general features useful for discrimination.

Optimization has been performed in three most significant variables: 1) The transverse mass produced by the lepton and  $E_T^{miss}$ ,  $m_T^{lep}$ ; 2) The angular difference between the  $b$ -jet and the  $E_T^{miss}$ ,  $(\Delta\phi(E_T^{miss}, p_T(b\text{-jet})))$ ; and 3) The ratio variable  $R_M$  that is defined as the ratio between  $E_T^{miss}$  and the transverse momentum of the leading jet  $p_T(j_0)$  [68],

$$R_M = \frac{E_T^{miss}}{p_T(j_0)}. \quad (3)$$

### 3.4 Signal extraction with ML

In order to discriminate signal from SM backgrounds in *stop* decay processes, a more complex approach based on ML techniques is performed. The objective is to design a statistical method capable of learning from several traits of backgrounds and signal samples in the multi-dimensional space defined by the features considered for this analysis. We can address the problem by using a binary classifier that categorizes between signal and background classes.

For our classification task, we train and evaluate a set of four ML algorithms that have different mathematical foundations. First, a logistic regression (LR) classifier [50] that basically is a statistical model based on regression analysis in which a dependent binary variable is fitted using a logistic model [69]. Second, we have chosen the Random Forest (RF) [51] and the Gradient Boosting Classifiers [52], which are sets of ensemble methods used to improve the performance of single classifiers [70]. On this regard, the Random Forest is fundamentally a bagging ensemble of decision trees [71], while the Optimized Gradient Boosting Classifier (XG) is a meta-model that iterates over a set of weak classifiers [72]. Finally, we propose a feed-forward Neural Network [53] intended to build a decision boundary after stacking several hidden layers of non-linear relationships [73]. It is important to remark that the difference in mathematical nature of the proposed classifiers let us grasp the traits of the latent space inherent to signal and background distributions.

Additionally, with the aim of covering a wider range of ML algorithms, we also attempted to perform the signal extraction with a Support Vector Machine (SVM) classifier. However, as the complexity of SVM scales at least quadratically with the number of training events [74, 75], we studied this classifier with a low number of training events, verifying that the computational time scales quadratically with the training events. Additionally, significance values obtained with the SVM showed to be around 5% better than the LR technique but lower than the RF and XGBoost algorithms, around 2% and 5% respectively. we have not included this approach in our study due to its practical limitations and performance similar to other ML algorithms in the preliminary tests.

Regarding the details for each proposed classifier, for the Logistic Regression we propose a logit regression model with a L2 regularization, which adds a squared penalization to

model coefficients [76]. We use regularization in order to reduce the over-fitting and improve numerical stability during the training phase. For the Random Forest [51], we propose a forest with 50 trees, Gini Impurity metric for splits and bootstrap [77]. The number of trees for the Random Forest classifier was chosen using a grid-search over the number of estimators in the model. Regarding the selection of these parameters for the RF classifier, we use the Gini impurity because it is less intensive than other split criteria when splitting nodes in decision trees.

For the Optimized Gradient Boosting, we use an ensemble of 100 trees boosted using the tree booster (*gbtree*). The number of the trees in this model was chosen after a grid-search where the significance was optimized. In that sense, each decision tree has 100 estimators. Furthermore, we chose a tree booster because we are iterating over weak decision trees [52]. Notice that a XGBoost is also an ensemble classifier like Random Forest. However, the XGBoost is based on boosting weak learners (shallow decision trees) that use gradient descent algorithms over the error metric. On the other hand, the random forest is a bagging of fully grown decision trees which are ensembled [70]. Finally, for the NN we propose a fully-connected NN with *Sigmoid* activation in the last layer and Rectified linear Units (*ReLU*) activation in previous layers [78]. The *Sigmoid* is commonly used for solving binary classification problems because it saturates when the argument (previous layers computation) is very positive or very negative. Note that *Sigmoid* behavior is needed as we aim to warranty the final layer to be insensitive to small changes in the saturation states. We performed a hyper-parameter optimization on the number of layers and nodes per layer. This optimization was carried out by comparing the validation accuracy for different configurations. In the case of the NN, we normalized the feature distributions fed to the neural network in order to remove the bias generated by any difference in the features dimensionality. Moreover, the feature normalization is needed to equally distribute the importance of all variables in the training phase. We tested different normalization techniques: Standardizing, Power Transform normalization and Quantile normalization [74]. The best improvement in significance was obtained when normalizing the features through a Quantile transformer algorithm with gaussian output.

## Features for ML Training

In supervised schemes, an ML model learns from specific features that belong to different classes with the aim of classifying a new sample. In the case of high-energy physics events, these features come from physical variables obtained after event reconstruction by the experiment. We have selected 12 of these variables from a wide set of low and high level features, knowing a priori that combining low and high level features maximizes the discriminatory power in the training [79]. In our study, low level features are variables that are reconstructed directly from the detector such as transverse momentum  $p_T$ , pseudo-rapidity  $\eta$  and azimuthal angle  $\phi$  of leptons, jets and  $b$ -jets. High level features come from a combination of low level variables, like differences between azimuthal angles of particles with respect to the  $E_T^{miss}$ , the ratio  $R_M$  (eq. 3) and the transverse mass of the lepton and  $E_T^{miss}$ ,  $m_T^{lep}$  (eq. 1). Since there is no standardized methodology to select the most adequate features for training, we have chosen this set of variables taking into account the value of significance given after training and evaluation over the whole data set. A list of the selected features is presented in Table 6. Histograms with distributions normalized to unity of all of these variables are shown in Figure 3. Here all backgrounds have been stacked together and the signal shown is a combination of the four benchmark signal masses, added in a proportional way to each

cross section. Some of these variables present a good discrimination between signal and background. For instance, the  $R_M$  and  $m_T^{lep}$  variables have contributions at high values in the SUSY signals due to large  $E_T^{miss}$  from the neutralinos in the SUSY benchmark points, compared to the backgrounds where the only source of  $E_T^{miss}$  comes mainly from the neutrinos and some leptons not reconstructed correctly in the final states. We can also note differences in several low level variables such as the pseudorapidity of the  $E_T^{miss}$ , the azimuthal difference between  $E_T^{miss}$  and lepton ( $\Delta\phi(E_T^{miss} - lep)$ ), and the azimuthal difference between  $E_T^{miss}$  and  $b$ -jet ( $\Delta\phi(E_T^{miss}, p_T(b\text{-jet}))$ ). The  $\eta(E_T^{miss})$  variable for the backgrounds tend to be in the forward region in contrast with the SUSY signal which is located in the central region due to the large contributions in  $E_T^{miss}$ . Furthermore, note that the  $\Delta\phi(E_T^{miss} - lep)$  variable implies that the lepton in the SUSY signal tends to be produced anti-parallel to the  $E_T^{miss}$ , whereas for the backgrounds that difference is approximately  $\frac{\pi}{2}$ . There is a discontinuity in the  $\Delta\phi(E_T^{miss}, p_T(b\text{-jet}))$  distribution that comes from the pre-selection  $\min \Delta\phi(j_{1,2}, E_T^{miss}) > 0.4$ .

Table 6: Physical variables used for training the ML classifiers.

Input Variable	Description
$E_T^{miss}$	Missing transverse energy
$\phi(lep)$	Azimuthal angle of the lepton
$\phi(E_T^{miss})$	Azimuthal angle of the $E_T^{miss}$
$H_T$	Scalar sum of the $p_T$ of jets
$p_T(\ell)$	Transverse momentum of the lepton
$p_T(j_0)$	Transverse momentum of the leading jet
$p_T(b\text{-jet})$	Transverse momentum of the $b$ -tagged jet
$\Delta\phi(E_T^{miss}, p_T(\ell))$	Azimuthal difference between $E_T^{miss}$ and $p_T(\ell)$
$\Delta\phi(E_T^{miss}, p_T(j_0))$	Azimuthal difference between $E_T^{miss}$ and $p_T(j_0)$
$\Delta\phi(E_T^{miss}, p_T(b\text{-jet}))$	Azimuthal difference between $E_T^{miss}$ and $p_T(b\text{-jet})$
$m_T^{lep}$	Transverse mass of the lepton and MET
$R_M$	Ratio between $E_T^{miss}$ and $p_T(j_0)$

## Data set and training

After a proton-proton collision, some of the final state observables are used for filtering some specific event topologies by the experimental triggers, which have certain features that enhance some particular physics processes which are of interest for the experiment. In our study, we are interested in events with at least one lepton (electron or muon) in the final state. Then, to target more specific events related to our final state configuration, we make the event pre-selection indicated in Table 3. Afterwards, we use the set of variables shown in Table 6 for the ML training. In principle, it has been shown that the more data for training the better the generalization a ML algorithm can achieve [80, 81]. However, in this paper we also consider the trade-off between the accuracy and the computational power needed to accomplish a desired performance. Consequently, due to computational constraints, we have a limited sample of 400000 events for training and  $150 \text{ fb}^{-1}$  for evaluation. We have performed a study on how the significance changes when we reduce the training sample, as shown in Figure 4, where we have selected the probability score that maximizes the significance for each algorithm. We have noticed a decreasing trend in significance as we reduce the training data set for all

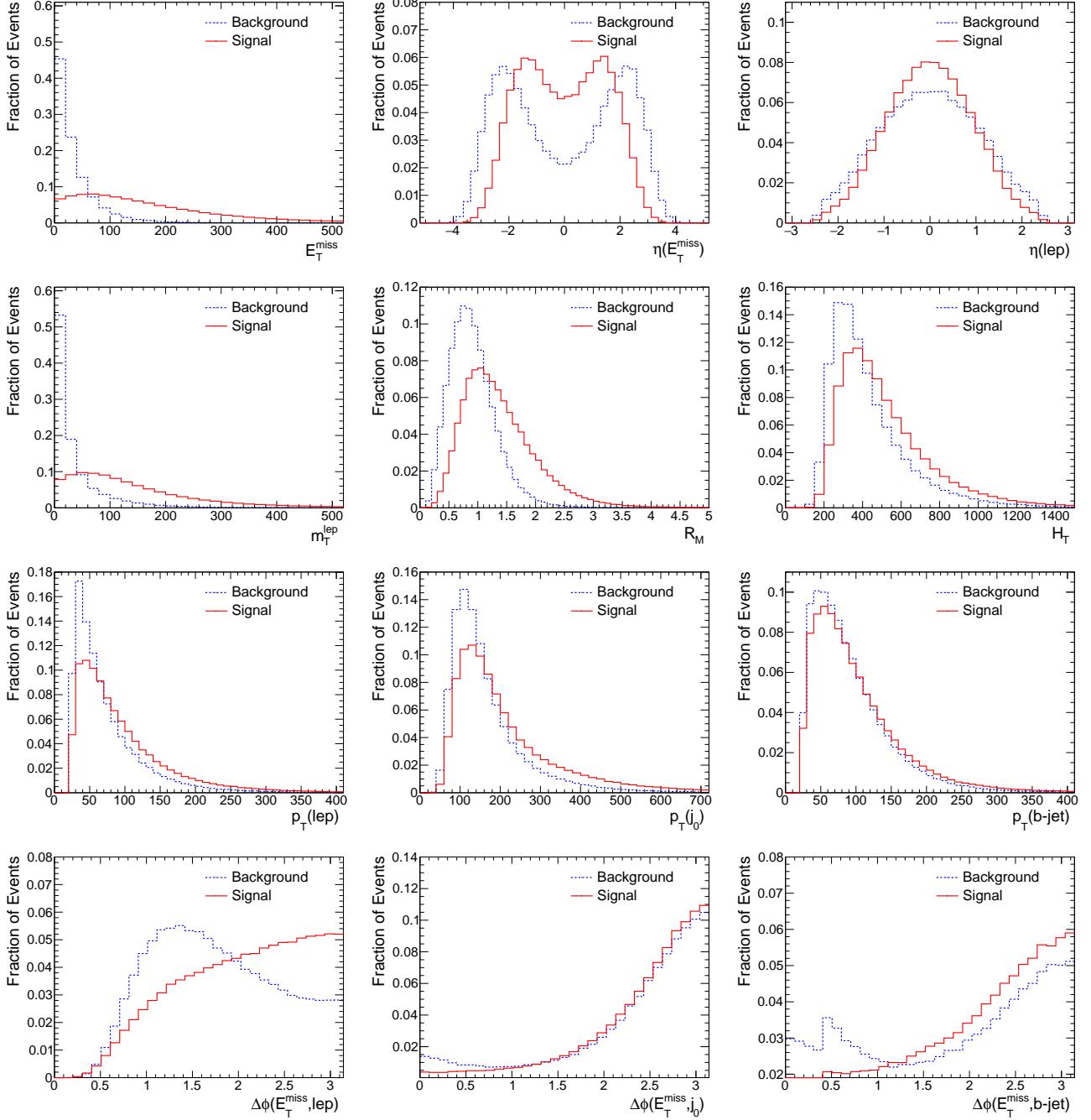


Figure 3: Distributions normalized to unity for signal and backgrounds used as feature inputs in the ML training. Here, all backgrounds have been stacked in one single histogram and the four benchmark signals have been added in a proportional way to their cross sections.

ML algorithms. The decreasing trend is much prominent for the NN. Therefore, the data set used for the ML training corresponds to the maximal set we have of 400000 events. The different sources of background are combined, according to the percentage contribution (given their cross sections), into one single background set equivalent to 50% of the total number of training events. The other 50% of training events corresponds to signal events. From the

total data set, 90% of the events have been used for training and 10% for testing. Background composition preserves the fractional contribution of each different background source after the baseline requirements. In the case of signal, we have taken all four benchmark samples in a single SUSY sample with events distributed in a proportional way to each benchmark cross section, so that there would be no bias in the training. In this sense, we have checked that the significance outcome is not affected significantly when training the ML algorithm with equal sets of each signal sample, for example 50000 events per signal benchmark. In such case, we have no major difference in the global significance calculated for all the benchmarks. Nevertheless differences in significance are observed for the highest benchmark mass  $s800$  with respect to our proposed way to mix the signal benchmarks, for instance, an increase of 2% and 10% for the NN and LR respectively, and a decrease of 4% and 28% for the XG and random forest respectively.

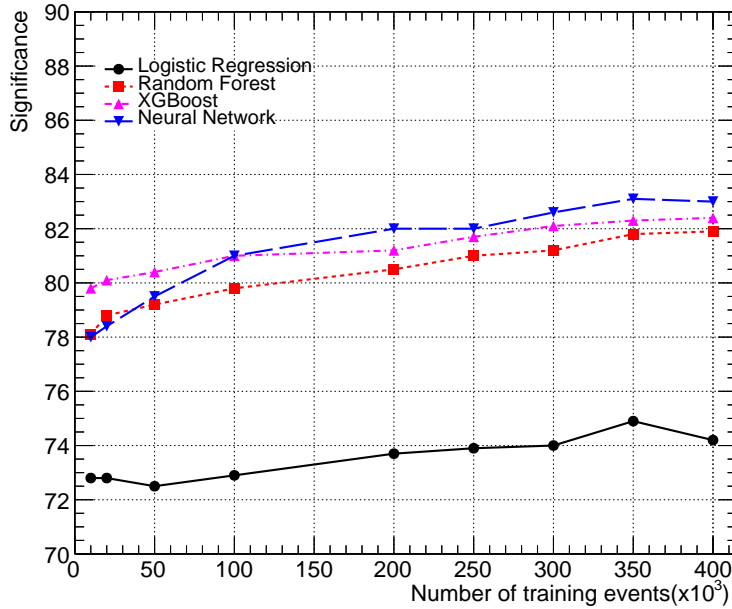


Figure 4: Significance as a function of the number of events in the training set for the four ML algorithms.

## 4 Results

### 4.1 Results for standard cut-and-count method

To maximize the discrimination of stop signal from backgrounds, we have analyzed the significance variation of several physical distributions, some of them shown in figure 3. We have found feasible to select events above 160 GeV in the  $m_T^{lep}$  distribution. This optimization can be verified in the upper panels of Figure 5. In the same way, we have found an optimal value of 0.8 for the ratio  $R_M$  [68] and this is shown in the middle panels of figure 5. Finally, a complementary requirement for the azimuthal angle between the  $E_T^{miss}$  and the  $b$ -jet  $p_T$  has

shown to reduce significantly the  $W$ +jets contributions. This can be seen in the lower panels of Figure 5. These selections are summarized in Table 7.

Table 7: Event selections for signal and backgrounds within the cut-and-count methodology.

$m_T^{lep}$	$> 160 \text{ GeV}$
$p_T(j_0)/E_T^{miss}$	$> 0.8$
$\Delta\phi(p_T^{b-jet}, E_T^{miss})$	$> 0.4$

After applying these selections, the final  $E_T^{miss}$  distribution is shown in the left panel of Figure 6. The last bin contains events above 1000 GeV. The variation of significance with respect to the selection in  $E_T^{miss}$  is shown in the right panel for each of the four benchmark points. A peak in this plot represents the maximum significance that can be achieved with the respective  $E_T^{miss}$  cut. Table 8 summarizes the selections in  $E_T^{miss}$  that maximize the significance for each signal benchmark. Note that these are the maximum significances that we can achieve using this methodology.

Table 8: Maximal significance expected for each signal benchmark point after applying the indicated  $E_T^{miss}$  requirement. Signal and background yields are shown for statistical reference.

	$E_T^{miss}$	Signal Events	Backgrounds							Sig.	$S/B$
	cut		$t\bar{t}$ 1L	$t\bar{t}$ 2L	$W$ +jets	ST	$t\bar{t}$ +V	VV	Total		
$s500$	210	4345	1043	1570	292	150	254	5	2763	49.2	1.6
$s600$	250	1291	540	695	151	76	159	1	1363	23.6	0.95
$s700$	300	442	258	260	75	38	88	1	612	12.7	0.72
$s800$	340	167	149	133	43	20	55	1	345	6.83	0.48

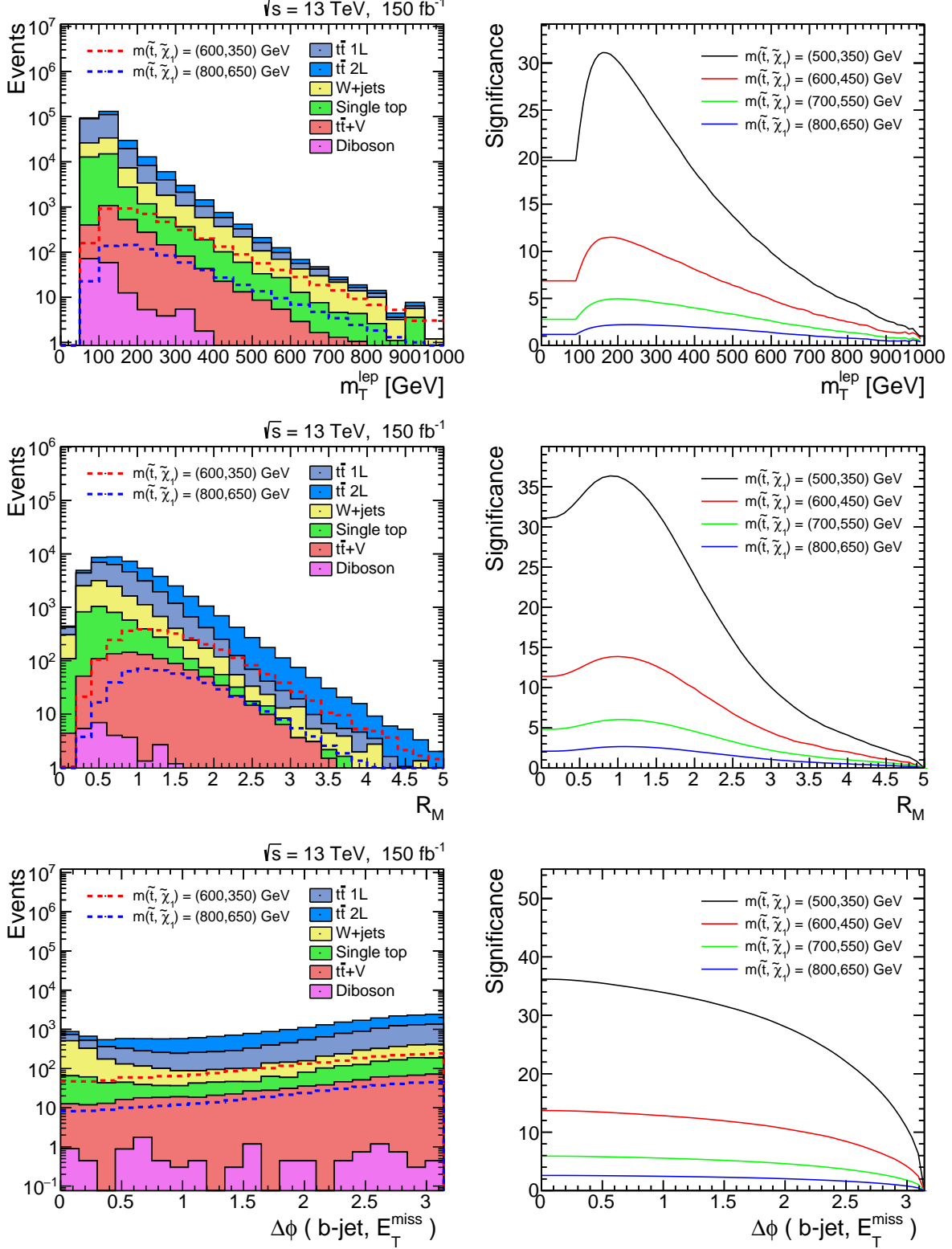


Figure 5: Optimization of significance for  $m_T^{\text{lep}}$  (upper panels) after pre-selection cuts,  $R_M$  (medium panels) after  $m_T^{\text{lep}} > 160 \text{ GeV}$  selection and  $\Delta\phi(\text{b-jet}, E_T^{\text{miss}})$  (lower panels) after  $m_T^{\text{lep}} > 160 \text{ GeV}$  and  $R_M > 0.8$ .



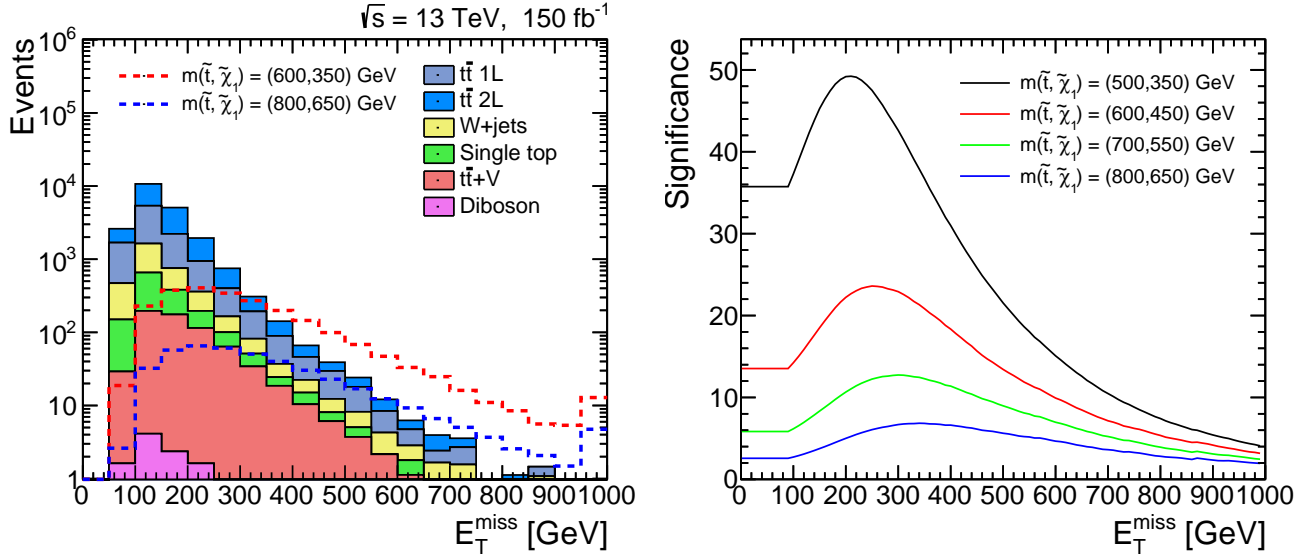


Figure 6: Event distribution for  $E_T^{miss}$  (left panel) and the significance of each benchmark as a function of the selection (right panel).

## 4.2 Results for ML algorithms

In this section, we study the performance of the previously defined ML classifiers for categorizing signal and SM backgrounds and their impact on the statistical significance, defined in Equation 2, on a testing sample.

### Training

Computations for the ML training were performed using servers with 31 Intel Xeon E5-2520 cores at 2.10GHz, and 32 GB of RAM memory. Meanwhile event simulations were carried out using 24 Intel Xeon E5-2640 cores at 2.50 GHz, and 65 GB of RAM memory. All neural networks were built using the Tensorflow [82] machine learning software libraries.

Each ML method has been tested with a subset corresponding to 10% of the main training data set of 400000 events. We have evaluated each algorithm with our main backgrounds and signal samples using the  $150 \text{ fb}^{-1}$  set. We have mentioned that for W+jets we have simulated only  $86.9 \text{ fb}^{-1}$  due to our limited computational capacity, so we have scaled only this background distribution to  $150 \text{ fb}^{-1}$ . Distributions of the probability score for the testing set for each of these ML methods are shown in Figure 7. Here, all backgrounds have been stacked and are shown in the blue shaded histogram. The *global* signal shown in the red shaded histogram is the sum of the four benchmarks stacked in a way proportional to their cross section. Note that the signal distribution has a peak for a probability score near unity.

From the distributions of Figure 7 we calculate the global significance, defined as the value obtained using the global signal stack. This is a first indicator of how the ML algorithm is separating signal events from backgrounds. The global maximum significance is displayed in Table 9 together with signal and background events for reference. The thresholds indicated are the probability score values where the significance gets its maximum for each benchmark. The evolution of the significance with respect to the threshold requirement is shown in Figure 8 for the four ML algorithms. Note that the NN and XGBoost algorithms have a similar behaviour and maxima.

Table 9: Global maximum significance obtained for each ML method.

	Threshold	Signal	Backgrounds	Significance
Logistic Regression	0.869	9827	6498	73.3
Random Forest	0.881	10267	4817	80.4
XGBoost	0.890	10310	4672	81.1
NN	0.889	10395	4704	81.5

Additionally, to complement the estimation of classification efficiency of each ML algorithm, in Figure 9 we show the receiving operating characteristic curves (ROC) [83]. The ROC curve is intended to show the relationship between the true positive rate and false positive rate at all classification thresholds. Furthermore, by measuring the area under the ROC curve (AUC) we estimate a scale and classification-threshold invariant metric to measure the model performance. Notice that AUC is equal to 1 when all the predictions are correct (i.e. no false positives nor false negatives). In that sense, in Figure 9 we have included the AUC metric for each classifier, noting that the best classification is performed by the NN algorithm.

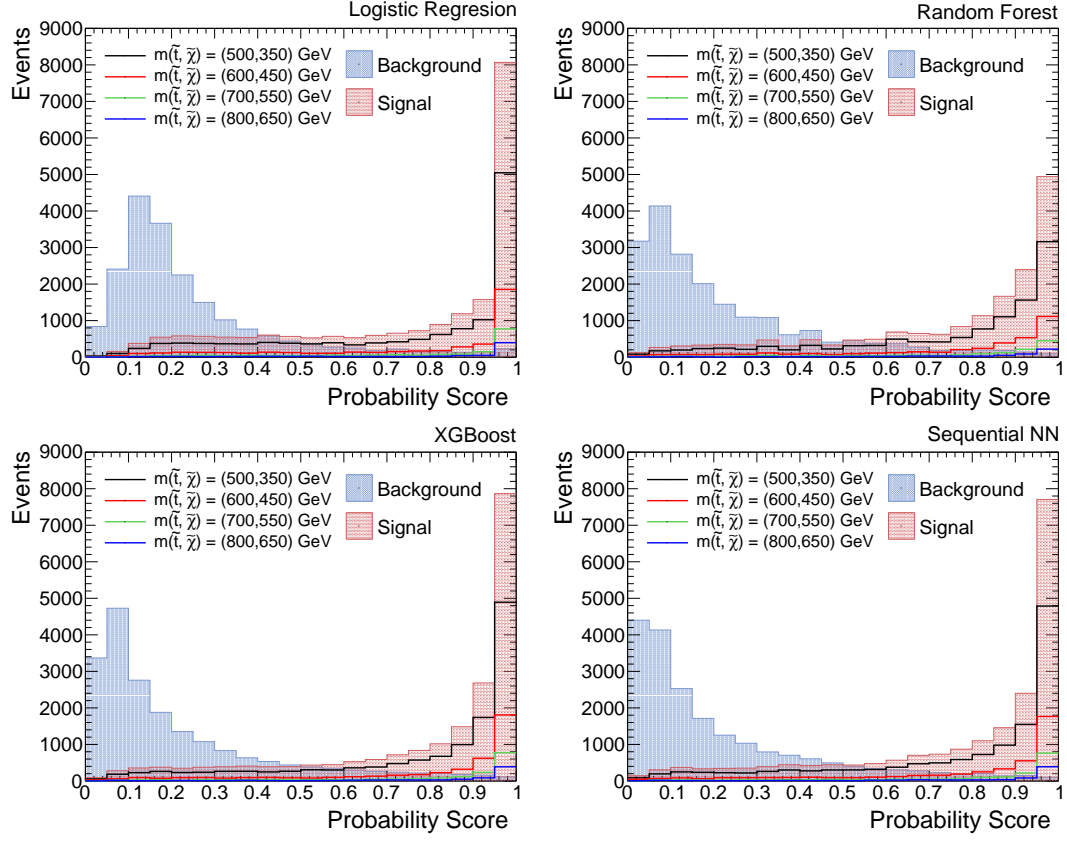


Figure 7: Probability score distributions for the testing set of events evaluated after the training for the logistic regression method (upper left), the random forest classifier (upper right), the XGBoost classifier (lower left) and a sequential NN (lower right).

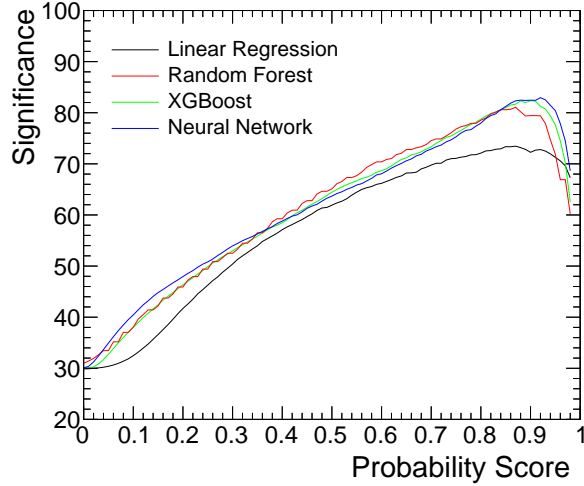


Figure 8: Significance as a function of the probability score for all ML algorithms.

## Evaluation

Using the same results for each ML algorithm, we split back the total signal into the original four sets corresponding to  $150 \text{ fb}^{-1}$  of each signal benchmark point. We calculate again the

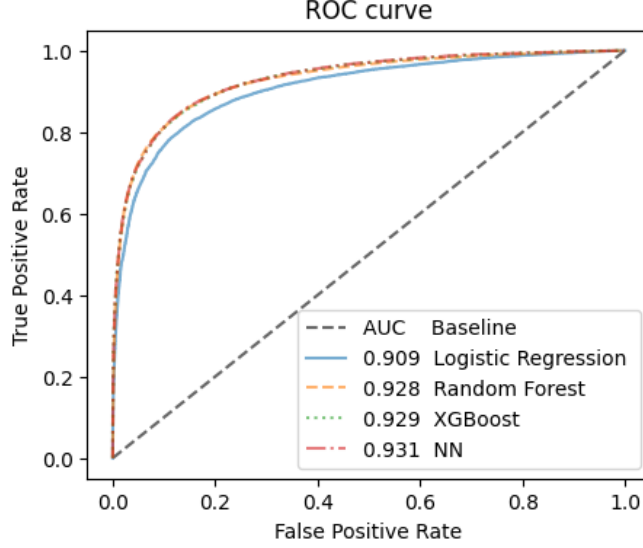


Figure 9: ROC curves and AUC values calculated for each ML method.

new thresholds that maximize the significance for each particular signal benchmark. In the left-hand panels of Figure 10 we present distributions of the probability score for all ML algorithms for the stacked backgrounds and two relevant benchmark points:  $s500$  and  $s800$ . In the right-hand panels, the significance as a function of the selection in probability score is presented, noting that the peak for each signal benchmark corresponds to a probability score close to unity. For the NN and XG algorithms, the probability score selection and calculation of significance is shown in Tables 10 and 11, respectively for each signal benchmark. Detailed event yields for backgrounds and signal benchmarks are given for reference.

Table 10: Maximal significance expected for each signal benchmark point after applying the respective probability score selection for the NN algorithm. Signal and detailed background yields are shown for statistical reference.

	Threshold	Signal	Backgrounds							Sig.	$S/B$
	cut	Events	$t\bar{t}$ 1L	$t\bar{t}$ 2L	$W$ +jets	ST	$t\bar{t}$ +V	VV	Total		
$s500$	0.910	6066	1080	1580	232	147	302	4	3585	59.1	1.7
$s600$	0.944	1917	546	717	115	78	190	3	2032	28.7	0.94
$s700$	0.979	547	235	276	62	36	126	0	535	15.7	1.0
$s800$	0.988	212	76	67	17	7	52	0	221	9.59	0.96

We make a comparison of the significances obtained through the standard cut-and-count methodology and the ones obtained using the ML algorithms for each signal benchmark. These results are summarized in Table 12 where the gain percentage columns come from the ratio between each ML algorithm significance and the ones obtained from the cut-and-count methodology.

Note that in Table 12, the gain in significance is consistently better for both the NN and XG classifiers, both of them providing equal improvement in significance within statistical uncertainties. The benchmark point  $s800$  shows a difference of 10% between the significance

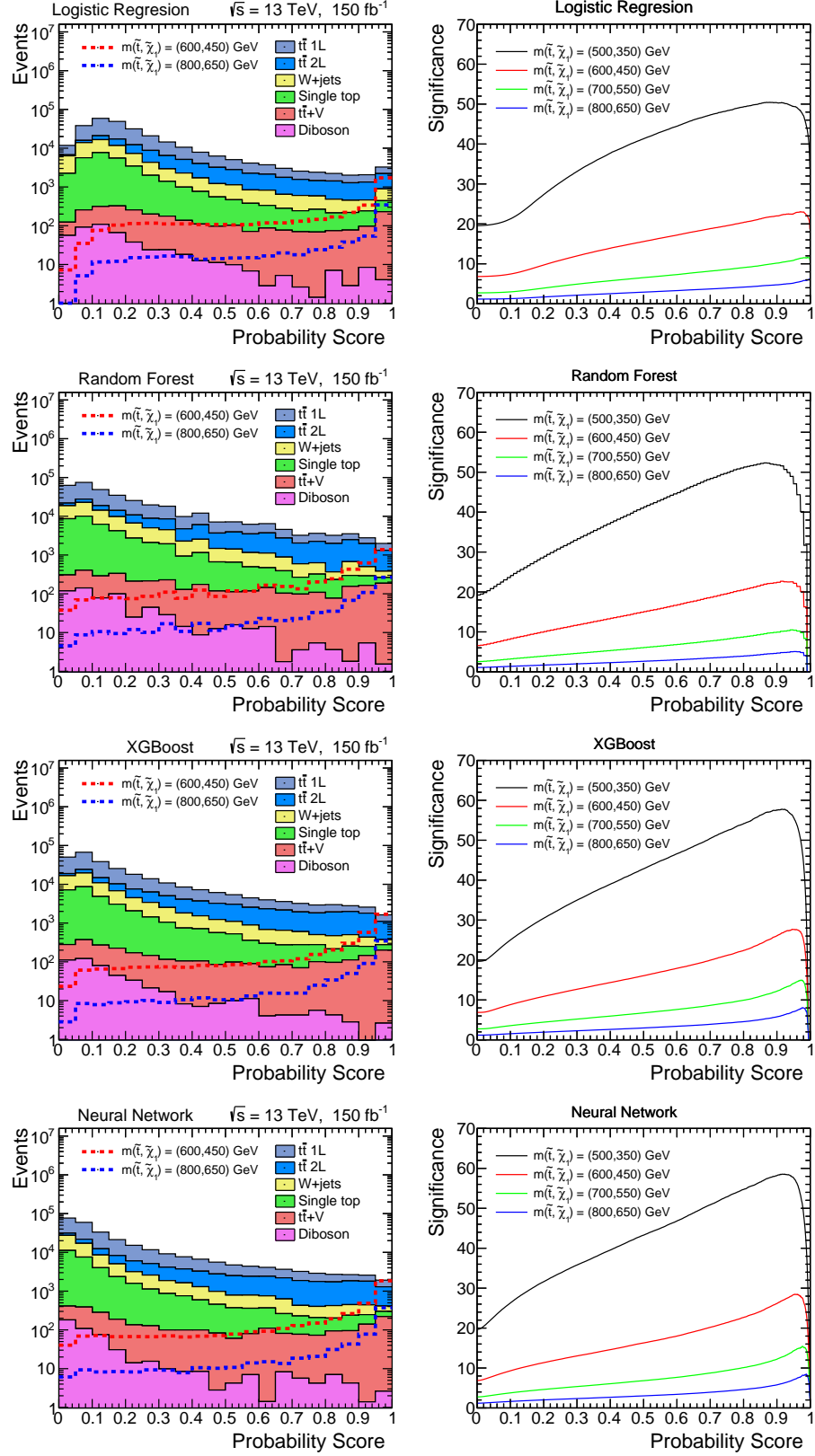


Figure 10: Probability score distributions (left panels) and significance variations as a function of the probability score cut (right panels) for all ML algorithms.

Table 11: Maximal significance expected for each signal benchmark point after applying the respective probability score selection for the XG algorithm. Signal and detailed background yields are shown for statistical reference.

	Threshold	Signal	Backgrounds								Sig.	$S/B$
	cut	Events	$t\bar{t}$ 1L	$t\bar{t}$ 2L	$W$ +jets	ST	$t\bar{t}$ +V	VV	Total			
$s500$	0.908	6069	1056	1689	244	148	293	3	3728	58.6	1.6	
$s600$	0.948	1813	605	832	112	89	216	3	1742	28.7	1.0	
$s700$	0.975	551	214	220	30	28	104	0	546	15.7	1.0	
$s800$	0.977	259	181	174	21	20	97	0	473	8.88	0.55	

Table 12: Gain in significance of the ML algorithms with respect to the traditional methodology.

Signal	Standard Methods	LR		RF		XG		NN	
$s500$	49.2	51.4	4%	57.7	17%	58.6	19%	59.1	20%
$s600$	23.6	24.5	4%	27.7	17%	28.7	22%	28.7	22%
$s700$	12.7	12.3	-3%	14.3	12%	15.7	23%	15.7	23%
$s800$	6.83	7.55	10%	7.84	14%	8.88	30%	9.59	40%

enhancement provided by these two algorithms, however, when comparing the number of signal and background events remaining after the applied threshold, as indicated in tables 10 and 11, the uncertainty is about 12%, making them statistically compatible.

## 5 Summary and conclusions

Four ML classifiers (a Logistic Regression, a Random Forest, an XGBoost and a NN) were implemented to study their potential in discriminating hypothetical SUSY signals from their corresponding SM backgrounds. The study is based on MC simulations of proton-proton collisions at  $\sqrt{s} = 13$  TeV considering a total integrated luminosity of  $150 \text{ fb}^{-1}$ , focusing on stop pair production with three-body decay ( $\tilde{t} \rightarrow bW\tilde{\chi}_1^0$ ) in a compressed spectra scenario, with final states of one isolated lepton, jets, and  $E_T^{miss}$ . To target the exclusion limit of the stop-neutralino mass phase-space reached by ATLAS and CMS experiments with the integrated luminosity gathered in the LHC run II [41, 42], four MSSM benchmark points were considered, with stop masses between 500 GeV and 800 GeV and neutralino masses 150 GeV lower, such that the decay of the stops is produced via an off-shell top quark intermediate state.

All four ML algorithms were trained with a common set of six low-level variables (corresponding to reconstructed  $p_T$  of final objects,  $E_T^{miss}$  and angular information of lepton and  $E_T^{miss}$ ) and six high-level variables (azimuthal difference of  $E_T^{miss}$  and other final objects, transverse mass of the final lepton and  $E_T^{miss}$ , scalar addition of  $p_T$  of all jets, and the ratio of  $E_T^{miss}$  to the  $p_T$  of the leading jet). For training, we have applied a selection in  $E_T^{miss}$  greater than 90 GeV, which is much lower than ATLAS and CMS experiment studies that apply selections of 230 GeV and 250 GeV, respectively. Therefore, we include more backgrounds, implying that our analysis is not biased towards SUSY higher mass spectra. A study of the optimal size of the training set of events was executed, and performance of the ML algorithms was measured in terms of signal to background significance. Additionally, to quantify any

enhancement in signal significance provided by the ML algorithms, a standard cut-and-count based analysis was implemented, following a similar approach of previous studies performed by ATLAS and CMS experiments in the channel of study.

With respect to discrimination, the conclusion is that all four ML algorithms have better performance in separating the studied SUSY compressed stop signals from backgrounds, when compared to a standard methodology based on accumulative selections. The NN and XGboost techniques compete with each other as the ones with the highest signal significance, having similar enhancement, within statistical uncertainties, and an overall improvement over 20% with respect to the standard cut-and-count methodology. The close performance between NN and XG algorithms was also anticipated by the study of the ROC distributions which were very similar for both of them, as it is shown in Figure 9. It is noteworthy that the final number of signal events selected by both NN and XG, after applying a threshold on the probability score that maximizes significance, is over 25% higher than the cut-and-count method, providing higher statistical power which is important at the time of establishing any exclusion limit. The competing performance of the algorithm based on Gradient boosting, as compared to NN, makes it very attractive due to the fact that these algorithms usually require less amount of data to converge, as shown in Figure 8. Furthermore, the XGBoost is much simpler to implement than the NN, as less hyper-parameters need to be optimized. For instance, in order to develop our NN we optimized the learning rate, the number of hidden layers, the number of neurons in each hidden layer and the optimizer, while for the XGBoost only the *eta* (step size) and *gamma* (minimum reduction to perform a further partition) were optimized. The results obtained in the present study demonstrate the high potential and improvement of the ML algorithms, specially NN and XG, as an efficient alternative and consistent tool for searching for physics BSM. We have proven that they could have a substantial impact in the SUSY compressed phase space, which is experimentally more challenging in separating signal and background.

## 6 Acknowledgements

We acknowledge financial support by the ministry of science and innovation of Colombia under contract number 80740-164-2021. We also thank the financial support of the faculty of science and the department of Physics of Universidad de Los Andes, Colombia.

## References

- [1] *Preface to Special Issue on “Learning to Discover”*, [Int. J. Mod. Phys. A](#), **33**, (2020)
- [2] Y. LeCun, Y. Bengio, G. Hinton, *Deep Learning*, [Nature](#), **521**, (2015)
- [3] D. Guest, K. Cranmer, D. Whiteson, *Deep Learning and its Application to LHC Physics*, [Annual Review of Nuclear and Particle Science](#), **68**, (2018) [[arXiv:1806.11484 \[hep-ex\]](#)]
- [4] A. Larkoski, I. Mout, B. Nachman, *Jet Substructure at the Large Hadron Collider: A Review of Recent Advances in Theory and Machine Learning*, [Phys. Rept.](#), **841**, (2020) [[arXiv:1709.04464 \[hep-ph\]](#)]
- [5] M. Ali, N. Badrud’din, H. Abdullah, F. Kemi, *Alternate methods for anomaly detection in high-energy physics via semi-supervised learning*, [Int. J. Mod. Phys. A](#), **35**, (2020)



- [6] S. Appel, W. Geithner, S. Reimann, M. Sapinski, R. Singh et al. *Application of nature-inspired optimization algorithms and machine learning for heavy-ion synchrotrons*, [Int. J. Mod. Phys. A](#), **34**, (2019)
- [7] T. Likhomanenko, P. Ilten, E. Khairullin, A. Rogozhnikov, A. Ustyuzhanin, M. Williams, *LHCb Topological Trigger Reoptimization*, [J. Phys. Conf. Ser.](#), **664**, 8, (2015) [[arXiv:1510.00572 \[physics.ins-det\]](#)]
- [8] D. Belayneh et al, *Calorimetry with Deep Learning: Particle Simulation and Reconstruction for Collider Physics*, [Eur. Phys. J. C](#), **80**, 7, (2020) [[arXiv:1912.06794 \[physics.ins-det\]](#)]
- [9] L. de Oliveira, M. Kagan, L. Mackey, B. Nachman, A. Schwartzman, *Jet-Images – Deep Learning Edition*, [JHEP](#), **07**, (2016) [[arXiv:1511.05190 \[hep-ph\]](#)]
- [10] G. Kasieczka, T. Plehn, M. Russell, T. Schell, *Deep-learning Top Taggers or The End of QCD?*, [JHEP](#), **05**, (2017) [[arXiv:1701.08784 \[hep-ph\]](#)]
- [11] A. M. Yasser, T. A. Nahool, M. Anwar, C. Bowerman, G. A. Yahya, *A new machine learning approach for predicting the spectra of meson bound states*, [Int. J. Mod. Phys. E](#), **29**, (2020)
- [12] M. Borisyak, F. Ratnikov, D. Derkach, A. Ustyuzhanin, *Towards automation of data quality system for CERN CMS experiment*, [J. Phys. Conf. Ser.](#), **9**, (2017) [[arXiv:1709.08607 \[physics.data-an\]](#)]
- [13] M. Grigorieva, D. Grin, *Clustering error messages produced by distributed computing infrastructure during the processing of high energy physics data*, [Int. J. Mod. Phys. A](#), **36**, (2021)
- [14] D. Guest, K. Cranmer, D. Whiteson, *Deep Learning and its Application to LHC Physics*, [Ann. Rev. Nucl. Part. Sci.](#), **68**, (2018) [[arXiv:1806.11484 \[hep-ex\]](#)]
- [15] A. Hoecker et al, *TMVA - Toolkit for Multivariate Data Analysis*, [arXiv:physics/0703039 \[physics.data-an\]](#)
- [16] The CMS collaboration, *Energy calibration and resolution of the CMS electromagnetic calorimeter in pp collisions at  $\sqrt{s} = 7$  TeV*, [JINST](#), **8** (2013) [[arXiv:1306.2016 \[hep-ex\]](#)]
- [17] V. Kuznetsov, T. Li, L. Gionmi, D. Bonacorsi, T. Wildish, *Predicting dataset popularity for the CMS experiment*, [J. Phys. Conf. Ser.](#), **1**, (2016) [[arXiv:1602.07226 \[physics.data-an\]](#)]
- [18] M. Hushchyn, P. Charpentier, A. Ustyuzhanin, *Disk storage management for LHCb based on Data Popularity estimator*, [J. Phys. Conf. Ser.](#), **664**, 4, (2015) [[arXiv:1510.00132 \[cs.DC\]](#)]
- [19] The ATLAS collaboration, *Observation of a New Particle in the Search for the Standard Model Higgs Boson with the ATLAS Detector at the LHC*, [Phys. Lett. B](#), **716**, (2012) [[arXiv:1207.7214 \[hep-ex\]](#)]

- [20] The CMS collaboration, *Observation of a new boson at a mass of 125 GeV with the CMS experiment at the LHC*, *Phys. Lett. B*, **716**, (2012) [[arXiv:1207.7235 \[hep-ex\]](#)]
- [21] T. LeCompte, S. Martin, *Large Hadron Collider reach for supersymmetric models with compressed mass spectra*, *Phys. Rev. D*, **84**, (2011) [[arXiv:1105.4304 \[hep-ph\]](#)]
- [22] H. Dreiner, M. Krämer, J. Tattersall, *How low can SUSY go? Matching, monojets and compressed spectra*, *EPL*, **99**, 6, (2012) [[arXiv:1207.1613 \[hep-ph\]](#)]
- [23] J. Evans, Y. Kats, D. Shih, M. Strassler, *Toward Full LHC Coverage of Natural Supersymmetry*, *JHEP*, **07**, (2014) [[arXiv:1310.5758 \[hep-ph\]](#)]
- [24] J. Schechter, J.W.F. Valle, *Neutrino Masses in  $SU(2) \times U(1)$  Theories*, *Phys. Rev. D* **22**, 2227, (1980)
- [25] D. Clowe, M. Bradac, A. Gonzalez, M. Markevitch, S. Randall, C. Jones, D. Zaritsky, *A direct empirical proof of the existence of dark matter*, *Astrophys. J. Lett.*, **648**, (2006) [[arXiv:astro-ph/0608407](#)]
- [26] E. Copeland, M. Sami, S. Tsujikawa, *Dynamics of dark energy*, *Int. J. Mod. Phys. D*, **15**, (2006) [[arXiv:hep-th/0603057](#)]
- [27] C.D. Froggatt, H. Nielsen, *Hierarchy of Quark Masses, Cabibbo Angles and CP Violation* *Nucl. Phys. B*, **147**, (1979)
- [28] I. Antoniadis, N. Arkani-Hamed, S. Dimopoulos, G. Dvali, *New Dimensions at a Millimeter to a Fermi and Superstrings at a TeV*, *Phys. Lett. B*, **436**, (1998) [[arXiv:hep-ph/9804398](#)]
- [29] N. Arkani-Hamed, S. Dimopoulos, G. Dvali, *Phenomenology, Astrophysics and Cosmology of Theories with Sub-Millimeter Dimensions and TeV Scale Quantum Gravity*, *Phys. Rev. D*, **59**, (1999) [[arXiv:hep-ph/9807344](#)]
- [30] A.R. Vieira, B. Hiller, M.C. Nemes, M. Sampaio, *Naturalness and theoretical constraints on the Higgs boson mass*, *Int. J. Theor. Phys.*, **52**, (2013) [[arXiv:1207.4088 \[hep-ph\]](#)]
- [31] S. Martin, *A Supersymmetry Primer*, *Advanced Series on Directions in High Energy Physics*, **21**, (2010) [[arXiv:hep-ph/9709356](#)]
- [32] G. Farrar, P. Fayet, *Phenomenology of the Production, Decay, and Detection of New Hadronic States Associated with Supersymmetry*, *Phys. Lett. B*, **76**, (1976)
- [33] M. Dine, A. Nelson, *Dynamical Supersymmetry Breaking at Low Energies*, *Phys. Rev. D*, **48**, (1993) [[arXiv:hep-ph/9303230](#)]
- [34] L. Girardello, M.T. Grisaru, *Soft Breaking of Supersymmetry*, *Nucl. Phys. B*, **194**, (1982)
- [35] J. Alwall, P. Schuster, N. Toro, *Simplified Models for a First Characterization of New Physics at the LHC*, *Phys. Rev. D*, **79**, (2009) [[arXiv:0810.3921 \[hep-ph\]](#)]
- [36] D. Alves et al, *Simplified Models for LHC New Physics Searches*, *J. Phys. G*, **39**, (2012) [[arXiv:1105.2838 \[hep-ph\]](#)]

- [37] C. Brust, A. Katz, S. Lawrence, R. Sundrum, *SUSY, the Third Generation and the LHC*, [\*JHEP\*, \*\*03\*\*, \(2012\)](#) [[arXiv:1110.6670 \[hep-ph\]](#)]
- [38] G. Kane, C. Kolda, L. Roszkowski, J. Wells, *Study of Constrained Minimal Supersymmetry*, [\*Phys. Rev. D\*, \*\*49\*\*, \(1994\)](#) [[arXiv:hep-ph/9312272](#)]
- [39] Cheng, HC., Gao, C., Li, L. et al. *Stop Search in the Compressed Region via Semileptonic Decays*. [\*J. High Energ. Phys.\* \*\*2016\*\* 36 \(2016\)](#). [[arXiv:1604.00007](#)]
- [40] Sebastian Macaluso, Michael Park, David Shih & Brock Tweedie, *Revealing compressed stops using high-momentum recoils*, [\*J. High Energ. Phys.\* \*\*03\*\* 151 \(2016\)](#) [[arXiv:1506.07885v1](#)]
- [41] The ATLAS collaboration, *Search for new phenomena with top quark pairs in final states with one lepton, jets, and missing transverse momentum in pp collisions at  $\sqrt{s}=13$  TeV with the ATLAS detector*, [[arXiv:2012.03799 \[hep-ex\]](#)]
- [42] The CMS collaboration, *Search for direct top squark pair production in events with one lepton, jets, and missing transverse momentum at 13 TeV with the CMS experiment*, [\*JHEP\*, \*\*05\*\*, \(2020\)](#) [[arXiv:1912.08887 \[hep-ex\]](#)]
- [43] A. Radovic, M. Williams, D. Rousseau, M. Kagan, D. Bonacorsi, A. Himmel, A. Aurisano, K. Terao, T. Wongjirad, *Machine learning at the energy and intensity frontiers of particle physics*, [nature](#), **560**, 2018
- [44] D. Bourilkov, *Machine and Deep Learning Applications in Particle Physics*, [\*Int. J. Mod. Phys. A\*, \*\*34\*\*, \(2020\)](#) [[arXiv:1912.08245 \[physics.data-an\]](#)]
- [45] P. Baldi, P. Sadowski, D. Whiteson, *Searching for Exotic Particles in High-Energy Physics with Deep Learning*, [Nature Commun.](#), **5**, (2014) [[arXiv:1402.4735 \[hep-ph\]](#)]
- [46] M. Romao, N. F. Castro, R. Pedro, *Finding New Physics without learning about it: Anomaly Detection as a tool for Searches at Colliders*, [[arXiv:2006.05432 \[hep-ph\]](#)]
- [47] T. Roxlo, M. Reece, *Opening the black box of neural nets: case studies in stop/top discrimination* [[arXiv:1804.09278 \[hep-ph\]](#)]
- [48] J. Guo, J. Li, T. Li, F. Xu, W. Zhang, *Deep learning for the R-parity violating supersymmetry searches at the LHC*, [\*Phys. Rev. D\*, \*\*98\*\*, \(2018\)](#) [[arXiv:1805.10730 \[hep-ph\]](#)]
- [49] A. Alves, *Stacking machine learning classifiers to identify Higgs bosons at the LHC*, [Journal of Instrumentation](#), **12** 05 (2017) [[arXiv:1612.07725 \[hep-ph\]](#)]
- [50] J. Carifio, J. Halverson, D. Krioukov, B. Nelson, *Machine Learning in the String Landscape*, [\*JHEP\*, \*\*09\*\*, \(2017\)](#) [[arXiv:1707.00655 \[hep-th\]](#)]
- [51] L. Breiman, *Random Forests*, [Machine Learning](#), **45**, 1, (2001)
- [52] T. Chen, C. Guestrin, *XGBoost: A Scalable Tree Boosting System*, [Association for Computing Machinery](#), (2016) [[arXiv:1603.02754 \[cs.LG\]](#)]

- [53] P. Baldi, K. Bauer, C. Eng, P. Sadowski, D. Whiteson, *Jet Substructure Classification in High-Energy Physics with Deep Neural Networks*, [\*Phys. Rev. D\*, \*\*9\*\*, \(2016\)](#) [[arXiv:1603.09349 \[hep-ex\]](#)]
- [54] Alwall, J., Frederix, R., Frixione, S. et al, *The automated computation of tree-level and next-to-leading order differential cross sections, and their matching to parton shower simulations*, [\*JHEP\*, \*\*07\*\*, \(2014\)](#) [[arXiv:1405.0301](#)]
- [55] J. Alwall, M. Herquet, F. Maltoni, O. Mattelaer, T. Stelzer, *MadGraph 5: Going Beyond*, [\*JHEP\*, \*\*06\*\*, \(2011\)](#) [[arXiv:1106.0522 \[hep-ph\]](#)]
- [56] Torbjörn Sjöstrand et al, *An Introduction to PYTHIA 8.2*, [\*Comput. Phys. Commun.\*, \*\*191\*\*, \(2015\)](#) [[arXiv:1410.3012\[hep-ph\]](#)]
- [57] The DELPHES 3 collaboration, J. de Favereau, C. Delaere, P. Demin, A. Giammanco, V. Lemaître, A. Mertens, M. Selvaggi, *DELPHES 3: a modular framework for fast simulation of a generic collider experiment*, [\*JHEP\*, \*\*02\*\*, \(2014\)](#) [[arXiv:1307.6346 \[hep-ex\]](#)]
- [58] Matteo Cacciari, Gavin P. Salam, Gregory Soyez, *The anti- $k_t$  jet clustering algorithm* [\*J. High Energ. Phys.\* \*\*0804\*\*: 063 \(2008\)](#) [[arXiv:0802.1189](#)]
- [59] Matteo Cacciari and Gavin P. Salam, *Dispelling the  $N_{63}$  myth for the  $k_t$  jet-finder*, [\*Phys. Lett. B\* \*\*641\*\* 57 \(2006\)](#) [[arXiv:hep-ph/0512210](#)]
- [60] CMS Collaboration, S. Chatrchyan, *The CMS Experiment at the CERN LHC*, [\*JINST\*, \*\*3\*\*, \(2008\)](#)
- [61] B. C. Allanach, *SOFTSUSY: a program for calculating supersymmetric spectra*, [\*Comput. Phys. Commun.\*, \*\*143\*\*, \(2002\)](#) [[arXiv:hep-ph/0104145](#)]
- [62] C. Borschensky et al, *Squark and gluino production cross sections in pp collisions at  $\sqrt{s} = 13, 14, 33$  and 100 TeV*, [\*Eur. Phys. J. C\*, \*\*74\*\*, \*\*12\*\*, \(2014\)](#) [[arXiv:1407.5066 \[hep-ph\]](#)]
- [63] L. A. Harland-Lang, A. D. Martin, P. Motylinski, R.S. Thorne, *Parton distributions in the LHC era: MMHT 2014 PDFs*, [\*Eur. Phys. J. C\*, \*\*75\*\*, \*\*5\*\*, \(2015\)](#) [[arXiv:1412.3989 \[hep-ph\]](#)]
- [64] ATLAS Collaboration, *Studies on top-quark Monte Carlo modelling with Sherpa and MG5aMC@NLO*, [ATL-PHYS-PUB-2017-007](#), (2017)
- [65] ATLAS Collaboration, *Jet energy scale measurements and their systematic uncertainties in proton-proton collisions at  $\sqrt{s}=13$  TeV with the ATLAS detector*, [\*Phys. Rev. D\*, \*\*96\*\*, \(2017\)](#) [[arXiv:1703.09665 \[hep-ex\]](#)]
- [66] ATLAS Collaboration, *Performance of missing transverse momentum reconstruction with the ATLAS detector using proton-proton collisions at  $\sqrt{s} = 13$  TeV*, [\*Eur. Phys. J. C\*, \*\*78\*\*, 2018](#) [[arXiv:1802.08168 \[hep-ex\]](#)]
- [67] ATLAS Collaboration, *ATLAS  $b$ -jet identification performance and efficiency measurement with  $t\bar{t}$  events in pp collisions at  $\sqrt{s}=13$  TeV*, [\*Eur. Phys. J. C\*, \*\*79\*\*, \(2019\)](#) [[arXiv:1907.05120 \[hep-ex\]](#)]

- [68] Haipeng An & Lian-Tao Wang, *Opening Up the Compressed Region of Top Squark Searches at 13 TeV LHC*, [Phys. Rev. Lett. \*\*115\*\*, 181602, \(2015\) \[arXiv:1506.00653\]](#)
- [69] A. Alves, *Stacking machine learning classifiers to identify Higgs bosons at the LHC*, [JINST, \*\*12\*\*, 05, \(2017\) \[arXiv:1612.07725 \[hep-ph\]\]](#)
- [70] O. Sagi L. Rokach, *Ensemble learning: A survey*, Wiley Inter-disciplinary Reviews: Data Mining and Knowledge Discovery, 8(4), e1249. [Wiley Online Library](#), (2018)
- [71] T. Oshiro, P. Perez, J. Baranauskas, *How Many Trees in a Random Forest?*, [International Workshop on Machine Learning and Data Mining in Pattern Recognition](#), (2012)
- [72] L. Mason , J. Baxter , P. Bartlett , M. Frean, *Boosting Algorithms as Gradient Descent*, [International Conference on Neural Information Processing](#), (1999)
- [73] I. Goodfellow, Y. Bengio, A. Courville, *Deep Learning*, Cambridge: MIT press. [mitpress](#), (2016)
- [74] F. Pedregosa et al, *Scikit-learn: Machine Learning in Python*, [[arXiv:1201.0490 \[cs.LG\]](#)]
- [75] Y. Zhang, *Support Vector Machine Classification Algorithm and Its Application*, [International Conference on Information Computing and Applications](#), (2012)
- [76] F. Salehi, E. Abbasi, B. Hassibi, *The Impact of Regularization on High-dimensional Logistic Regression*, [[arXiv:1906.03761 \[stat.ML\]](#)]
- [77] L. Raileanu, K. Stoffel, *Theoretical Comparison between the Gini Index and Information Gain Criteria*, [Annals of Mathematics and Artificial Intelligence](#), **41**, (2004)
- [78] V.Nair, G.Hinton, *Rectified linear units improve restricted boltzmann machines*, [International Conference on Machine Learning](#), (2010)
- [79] J. Heaton, *An Empirical Analysis of Feature Engineering for Predictive Modeling*, [IEEE Xplore](#), (2016) [[arXiv:1701.07852 \[cs.LG\]](#)]
- [80] C. Sun, A. Shrivastava, S. Singh, A. Gupta, *Revisiting Unreasonable Effectiveness of Data in Deep Learning Era*, [2017 IEEE International Conference on Computer Vision \(ICCV\)](#), (2017) [[arXiv:1707.02968 \[cs.CV\]](#)]
- [81] Joel Hestness et al, *Deep Learning Scaling is Predictable, Empirically*, [[arXiv:1712.00409 \[cs.LG\]](#)]
- [82] M. Abadi, A. Agarwal, P. Barham, E. Brevdo, Z. Chen et al, *TensorFlow: Large-Scale Machine Learning on Heterogeneous Distributed Systems*, [[arXiv:1603.04467 \[cs.DC\]](#)]
- [83] K. Feng, H. Hong, K. Tang, J. Wang, *Decision Making with Machine Learning and ROC Curves*, [[arXiv:1905.02810 \[stat.ME\]](#)]